Gravitational waves from strongly magnetised neutron stars

Paul D Lasky[1], Burkhard Zink and Kostas D Kokkotas

Theoretical Astrophysics, Institute for Astronomy and Astrophysics, University of Tübingen, Auf der Morgenstelle 10, Tübingen 72076, Germany

E-mail: paul.lasky@unimelb.edu.au

Abstract. Strongly magnetised neutron stars are prime candidates for multi-messenger astronomy given their proximity and regular, energetic flaring events. We present non-linear, ideal MHD simulations of strongly magnetised neutron stars in general relativity that are models for post-flare internal dynamics of these stars. In particular, magnetic field instabilities are used to trigger global reconfigurations of the magnetic field, which in turn excites both fluid and Alfvén modes throughout the star. These simulations are discussed in the context of gravitational wave emissions and detectability for ground-based gravitational wave detectors.

1. Introduction

Soft-gamma repeaters (SGRs) and anomalous X-ray pulsars (AXPs) are classes of neutron stars, collectively known as *magnetars*, that contain the most extreme magnetic fields in the Universe. These exotic objects exhibit sporadic bursting and flaring events, which are commonly associated to dynamics of the magnetic field. The strongest of these flares has been considered in the literature as possible multi-messenger gravitational wave sources, which has prompted targeted gravitational wave searches [1–5]. Presently, these searches have placed upper limits on gravitational wave energies of 1.4×10^{49} erg for the f-mode (i.e. in the kHz frequency range), and 3.5×10^{44} erg for white noise around $100 - 200$ Hz.

Comparatively little theoretical work has been done on the topic of magnetar flares as a viable source of gravitational radiation. In part this is due to a reasonably poor understanding of the internal dynamics of the objects during and immediately following a flare. Ioka [6] first investigated this question by looking at the maximum gravitational wave energy released by a change in moment of inertia induced by a dynamical rearrangement of the core magnetic field inside the star. They were able to place an upper limit of about 10^{49} erg under ideal conditions, including optimistic values of the internal magnetic field. More recently, Corsi & Owen [7] found similar values to be possible under more generic conditions, still tapping into the full energy reservoir associated with an instantaneous change in the magnetic potential energy of the star. In contrast, Levin & van Hoven [8] did not find f-mode detection to be very likely in the near future. Their model was based on some mechanism external to the star triggering the internal f-modes.

In this work we present details of recent theoretical work aimed at understanding these gravitational wave emissions caused by a large-scale rearrangement of the internal magnetic

[1] Current Address: School of Physics, University of Melbourne, Parkville, VIC 3010, Australia

field [9]. In particular, we utilise magnetic field instabilities to trigger global reconfigurations of the magnetic field, and determine the gravitational wave output for such models. Recently, Ciolfi *et al.* [10] performed numerical simulations of the same hydromagnetic simulations as our earlier paper [11], concluding that giant flares *could* give rise to observable gravitational radiation. However, they utilised a stellar model with a surface magnetic field strength some sixty times the strongest observed to reach these conclusions. We have shown [9] that the gravitational wave energy emitted in these events is a highly nonlinear function of the magnetic field strength, implying f-mode detection is unlikely.

This article provides a conglomeration of our two recent papers [9, 11]. In section 2 we briefly describe our model and numerical method. In section 3 we discuss the hydromagnetic instability that we elucidated in [11], and in section 4 we discuss the gravitational wave output and detectability of the signal.

2. Model

We study the time evolution of the ideal MHD equations in general relativity under the Cowling approximation utilising the three-dimensional GRMHD code THOR [12, 13] and her sister GPU code HORIZON [14]. The MHD portion of the code utilises the conservative formalism outlined in [15], with hyperbolic divergence cleaning employed following the prescription of ref. [16]. In the following simulations we use a Cartesian grid with 120^3 grid points. Resolution studies have been completed using 90^3, 150^3 and 200^3 grid points, finding consistent phenomenology. The outer boundary of our star is located approximately 1.4 times the stellar radius (at the closest point), and we adopt Dirichlet boundary conditions for the evolution of the magnetic field at this outer boundary. We have performed various tests with different boundary conditions and again found consistent phenomenology. For further specifics on the code and the numerical method we refer the reader to a forthcoming article [17].

The spectral code LORENE is utilised to create initial conditions, which are self-consistent solutions of the Einstein-Maxwell field equations in ideal MHD with purely poloidal magnetic fields[18]. Our fiducial model is a non-rotating star with polytropic equation of state relating the pressure, P, and rest-mass density, ρ, through $P = K\rho^{\Gamma}$, with $\Gamma = 2$ and $K = 100$. This gives a stellar model with gravitational mass $M = 1.3\,\mathrm{M}_{\odot}$ and equatorial radius $R = 12.6\,\mathrm{km}$.

3. Hydromagnetic Instabilities

Purely poloidal fields are known to be dynamically unstable to the kink instability from local, linear studies in Newtonian physics [19]. Such studies have been confirmed with global, linearised numerical evolutions [20] and in full non-linear studies [21]. Such configurations were also shown to be unstable in fully nonlinear relativistic calculations in Lasky *et al.* [11] – some details of which we repeat here.

The modal structure of the instability is extracted by performing a Fourier decomposition of the B_ϕ component of the magnetic field on a ring in the equatorial plane. We compute complex weighted averages

$$C_m\left(B_\phi\right) = \frac{1}{2\pi}\int_0^{2\pi} B_\phi\left(\varpi,\, \phi,\, z=0\right) \mathrm{e}^{im\phi} d\phi, \tag{1}$$

where $\varpi = \sqrt{x^2+y^2} = \text{const.}$ lies in the initial equatorial plane of the magnetic field. In figure 1 we plot the evolution of the $m = 1, \ldots, 4$ modes for $C_m\left(B_\phi\right)$ for an evolution with surface magnetic field $B_{\mathrm{surf}} = 8.8 \times 10^{15}\,\mathrm{G}$. These curves are extracted at a radius of $\varpi = 0.6\varpi_\star$, where $\varpi_\star$ is the stellar radius.

An instability can be seen in all modes after the first couple of Alfvén crossing times. Each mode grows exponentially by approximately six orders of magnitude over many subsequent Alfvén crossing times. Saturation of the modes is seen to occur after about 75 ms, at which

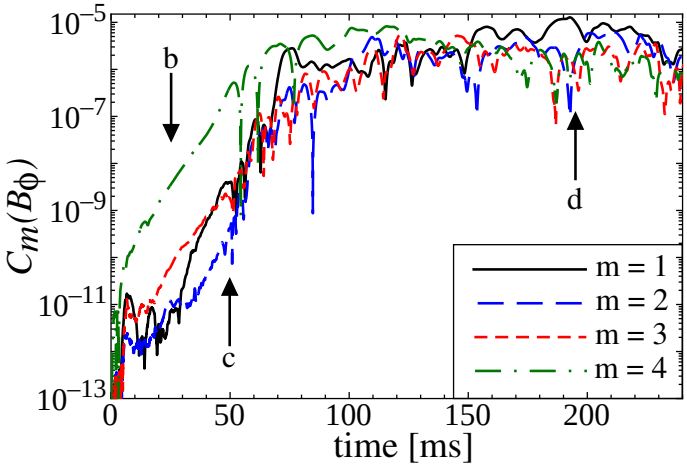

Figure 1. Evolution of $C_m\,(B_\phi)$ as a function of time for a model with initial surface magnetic field of $B_{\rm surf} = 8.8\times10^{15}$ G, yielding an Alfvén crossing time of 5.0 ms. The arrows represent the times of the three-dimensional snapshots plotted in figure 2. This figure was originally published in [11].

point the simulation evolves to a pseudo-equilibrium state. We have evolved such simulations to 400 ms $\equiv 80\,t_A$, where t_A is the Alfvén crossing time, with little variation in the equilibrium configuration following the first hundred or so milliseconds. The equilibrium configurations are discussed in more detail in refs. [11, 17].

In figures 2 we present three-dimensional plots of the magnetic field at various instances throughout the evolution. The instability acts near the neutral line, which is the line where $B = 0$ around the equatorial plane. In our simulations this is located at approximately two-thirds of the stellar radius. For clarity we have plotted red magnetic field lines seeded near the neutral line in the equatorial plane. Also plotted are black field lines seeded in the equatorial plane interior to the neutral line. The blue volume rendering is an isopycnic surface of $\rho = 0.37\rho_c$, where ρ_c is the central rest-mass density. This surface lies at a radius of approximately 50% of the stellar radius, which is well inside the neutral line.

Figure 2a shows the initial data imported from the LORENE spectral code. The domain of our grid is larger than that plotted here, and field lines are truncated at the surface of the star for clarity in the figure.

Figure 2b shows the evolution after 25 ms $\equiv 5\,t_A$. The onset of the "sausage" or "varicose" mode [19], involving a change in the cross-sectional area of a flux tube around the neutral line, is clearly visible. This is strongest in the $m = 4$ mode, which is a result of the transient excitation at the beginning of our simulation (for more details we refer the reader to ref. [11]). It is worth noting that, while this transient reduces with increasing grid resolution, the presence of the varicose mode is an inherent characteristic of the system.

Figure 2c shows the point at which the "kink" instability begins to visually dominate the system, which is after 50 ms $= 10\,t_A$. The kink mode acts perpendicularly to the gravitational field, in accordance with the prediction of ref. [19]. While one can still see the presence of the varicose mode in this snapshot, this point represents the non-linear development of the instability where the change in field structure is of similar order to the background field.

Figure 2d shows the simulation after 195 ms $= 39\,t_A$. This is a typical snapshot many Alfvén timescales after the non-linear saturation of the unstable modes. In some ways, this figure is consistent with the "twisted-torus" configurations seen in the non-linear evolutions of refs. [22, 23], and in the semi-analytic equilibrium calculations of refs. [24, 25]. Figure 2d shows about half of the star is well approximated by a twisted-torus, however the remainder of the star also exhibits large non-axisymmetric structures.

A way of classifying variation from the initial state is through calculating the relative energy in the toroidal and poloidal components of the magnetic field. In figure 3 we plot the evolution

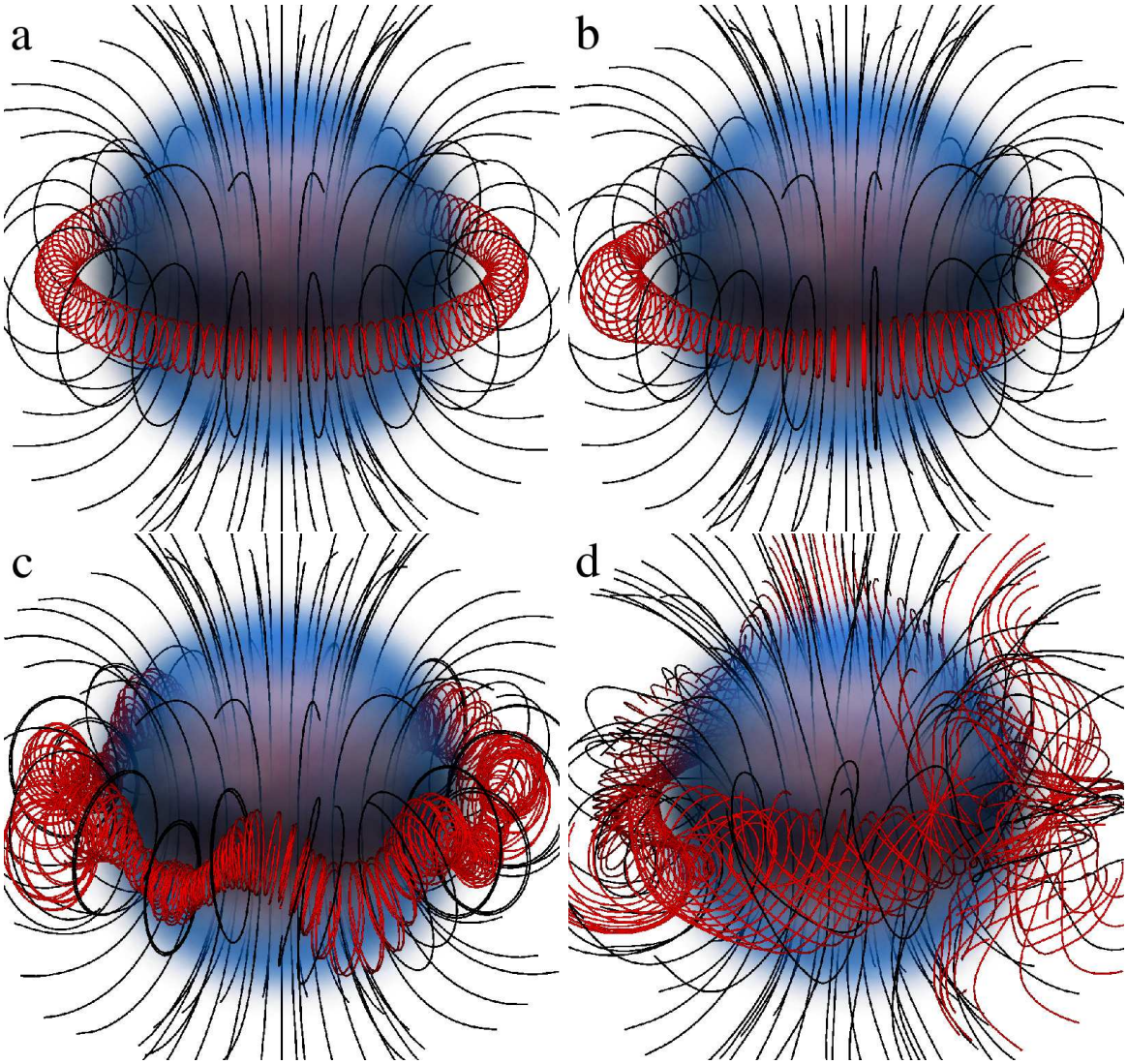

Figure 2. Time evolution of model in figure 1 with an Alfvén crossing time of 5.0 ms. The figures are (a) $t = 0$ ms, (b) $t = 25$ ms, (c) $t = 50$ ms and (d) $t = 195$ ms. The red magnetic field lines are seeded on the equatorial plane close to the neutral line to more clearly visualise the instabilities, while the black magnetic field lines are seeded on the equatorial plane interior to the neutral line. The volume rendering is an isopycnic surface at 37% of the central rest-mass density which is shown only to provide contrast with the field lines. A full movie of this simulation lasting 400 ms can be seen at www.tat.physik.uni-tuebingen.de/∼tat/grmhd. These figures were originally published in [11].

of the ratio of poloidal magnetic energy, E_p, to total magnetic energy, E, calculated inside the stellar radius. Numerous models are plotted here with polar magnetic fields between $B_{15} = 6$ to 55, where $B_{15} = B_{\rm surf}/10^{15}$ G. The temporal evolution is here normalised to the Alfvén crossing time of the system, showing that this is the dominant timescale for the evolution of the instability. It is worth stressing here that it takes between twenty to thirty Alfvén crossing times for the instability in the system to saturate. It can be seen from this plot that the equilibrium configurations are generically characterised by magnetic fields with $E_p/E \sim 0.65$. The relevance

of these results for neutron star physics are discussed in more detail in refs. [11, 17]

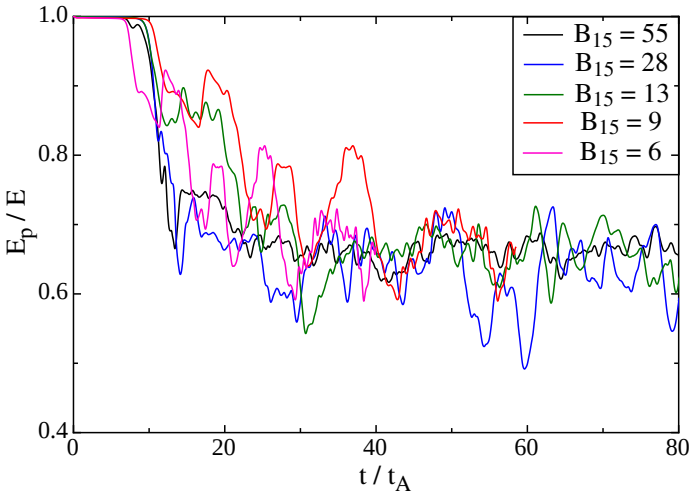

Figure 3. Evolution of the ratio of poloidal magnetic energy, E_p, to total magnetic energy, E, for models with varying magnetic field strengths, from $27\,B_{15}$ to $3.2\,B_{15}$, where $B_{15} = B_{\rm surf}/10^{15}$G. The evolutions here are normalised to the Alfveń crossing time of the system.

4. Gravitational Wave Emissions

The preceding simulations provide an invaluable tool for predicting gravitational wave emissions from magnetised neutron stars. In particular, we utilise the hydromagnetic instabilities to mimic a global magnetic field reconfiguring that may occur during, or immediately following, a magnetar flare. While the entire magnetic field may not rearrange in a realistic magnetar, rearranging the entire field gives us an *upper limit* of gravitational wave excitation in one of these events.

Our simulations exhibit negligible gravitational wave strain (i.e. $h_\times \lesssim 10^{-27}$ measured at 10 kpc) for the initial period of the simulation. During the non-linear phase of the instability, typically around $20\,t_A$ into the evolution, the gravitational wave strain grows until the instability saturates, at which point the strain signal remains roughly constant. More details of this can be seen in Zink *et al.* [9]. It is worth noting that the dominant mechanism for damping the f-mode is through gravitational wave emissions, which occurs on a timescale of order $100-200$ ms [26, 27]. As we are working in the Cowling approximation, we do not see such damping, and hence the gravitational wave amplitude remains nearly constant throughout the evolution of the system.

In figure 4 we show the gravitational wave amplitude as a function of surface magnetic field strength. The approximate values and error bars for the strains are derived from the time variation in the $h_\times$ signals (which are similar in amplitude to h_+) after the instability has saturated. We find an approximate power-law relation between h and $B_{\rm surf}$ given by

$$h \approx 1.1 \times 10^{-27} \left(\frac{10\,kpc}{d}\right) \left(\frac{B_{\rm surf}}{10^{15}\,{\rm G}}\right)^{3.3} . \qquad (2)$$

It is worth noting that the 3.3 exponent is an approximate value we find from this particular set of simulations. In general, this number will vary with the equation of state and magnetic field configuration, however an exponent of approximately 3 does agree with theoretical predictions. This will be explored in detail in a future article [17].

Most of the energy in the aforementioned signal is in the f-mode. Assuming a gravitational wave damping time of approximately 100 ms [26, 27], we find a corresponding power-law relation

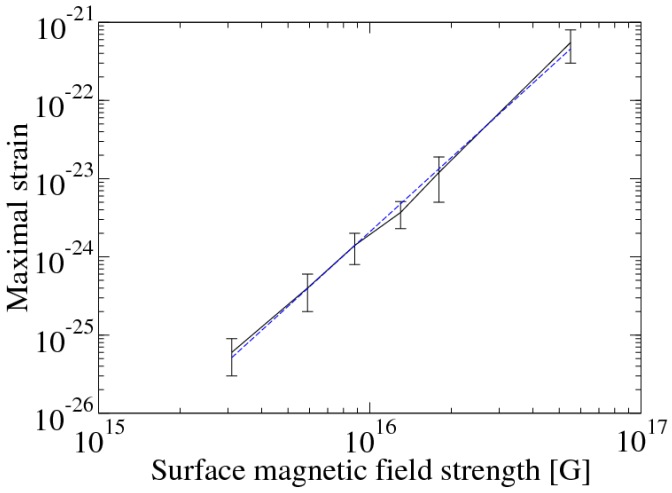

Figure 4. Gravitational wave strain as a function of surface magnetic field strength at the stellar pole. The signal amplitude is found to depend strongly on the magnetic field strength, ranging from almost 10^{-21} for our most extreme model down to less than 10^{-25} for models closer to realistic magnetar strengths. The dashed line is a power-law fit to the data – equation 2. This figure was originally published in [9].

for the energy emitted in gravitational wave radiation

$$E_{gw} \approx 1.5 \times 10^{36} \left(\frac{B_{\rm surf}}{10^{15}\,{\rm G}} \right)^{6.5} {\rm erg}. \tag{3}$$

We can see from the above two relations that the gravitational wave amplitude and energies are highly non-linear functions of the surface magnetic field strength. Moreover, for typical magnetar field strengths of order 10^{15} G, one finds strains *below* 10^{-25} and energies lower than 10^{40} erg for a source at 10 kpc, even if we assume a catastrophic global restructuring of the field to be associated with a giant flare.

We provide the signal-to-noise ratios for different detector sensitivity curves in figure 5. Here we have plotted the signal amplitude, $\sqrt{T}|\tilde{h}\,(f)\,|$, where T is the damping time of the oscillation and $\tilde{h}\,(f)$ is the Fourier transform of $h_\times$, as a function of the frequency for various magnetic field strength models. At approximately 1.8 kHz we show the signal amplitude for the f-mode as excited by the hydromagnetic instability assuming a damping time of 50 ms $\leq T \leq$ 200 ms. In the lower part of the spectrum we plot the other maximal mode seen in the Fourier transform, assuming a damping time between 10 ms $\leq T \leq$ 1 s. Over this we plot the entire spectrum (assuming $T = 100$ ms) for two models with $B_{\rm surf} = 8.8 \times 10^{15}$ G and $B_{\rm surf} = 1.8 \times 10^{16}$ G. Finally, we also plot the root of the noise power spectral density, $\sqrt{|S_h(f)|}$, as a function of frequency for the LIGO, AdvLIGO and ET detectors [28].

The amplitude signal-to-noise ratio, defined by $\sqrt{T}|\tilde{h}(f)|/\sqrt{|S_h(f)|}$, can be read off the graph as the ratio between the signal and the noise curve for the respective detector. The main conclusion from this figure is this: Assuming a giant flare is associated with a catastrophic large-scale rearrangement of the core magnetic field, *the gravitational wave signal associated with f-modes are not observable with present or near-future gravitational wave observatories* [9].

We do note the presence of lower frequency modes in the 10–100 Hz region of the spectrum. These are Alfvén modes, whereby the restoring force is provided by the magnetic field itself. The dominant damping mechanism for these modes is largely unknown, although it is generally expected that they will last significantly longer than the f-mode signal. For this reason we have plotted them in figure 5 with damping times between 10 ms and 1 s, although we note they may be excited for significantly longer than this. These modes are an exciting new prospect for gravitational wave detection [9], which we discuss in significantly more detail in a forthcoming article [17].

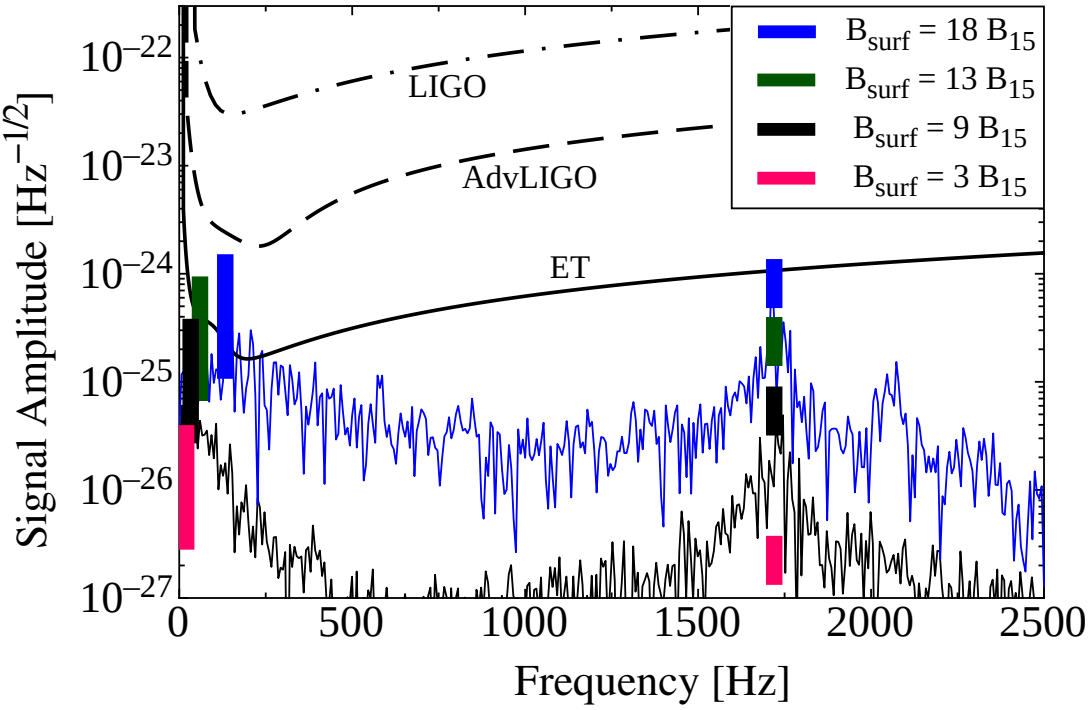

Figure 5. Signal amplitude, $\sqrt{T}|\tilde{h}(f)|$ against oscillation frequency. The coloured boxes on the right represent the maximum for the f-mode assuming a constant periodic source lasting between 50 and 200 ms. The coloured boxes on the left represent the maximum mode seen in the Fourier transform for any given frequency below the f-mode frequency assuming a constant periodic source lasting between $10\,ms$ and $1\,s$. These scale with $\sqrt{T}$, implying one can easily extrapolate to alternative values of the damping time. We have further plotted the entire spectrum (assuming a damping time of 100 ms) for both the $B_{\rm surf} = 1.8 \times 10^{16}$ G model (blue line) and $B_{\rm surf} = 8.8 \times 10^{15}$ G model (black line). This figure was originally published in [9].

5. Conclusion

We have performed three-dimensional, general relativistic magnetohydrodynamic simulations of neutron stars endowed with initially purely poloidal magnetic field geometries. This was achieved by evolving initially self-consistent solutions of the Einstein-Maxwell equations under the assumption of ideal MHD and the Cowling approximation. Purely poloidal magnetic field configurations are intrinsically unstable to the kink instability, which acted to reconfigure our internal magnetic field structure. This reconfiguring enabled us to investigate three separate phenomena: (i) the nature of the instability itself, (ii) the quasi-equilibrium configurations achieved as steady-state solutions and (iii) the gravitational wave emission from such magnetic field rearrangement. These have each been addressed in two previous papers [9, 11], and will be broached in more detail in a forthcoming article [17].

The most pertinent conclusions to be garnered from this work are two-fold: Firstly, that gravitational wave emissions associated with f-modes caused by the magnetic field rearrangement in a magnetar are not observable using current technologies. This is consistent with the conclusion of Levin & van Hoven [8] who argue that an *external* rearrangement of the magnetic field will not cause sufficient gravitational radiation for detection. The second, and significantly more speculative conclusion, is that lower frequency radiation – i.e. in the 10's to

100's of Hz range – may be detectable. The existence of modes at these frequencies is particularly intriguing given the detectors are most sensitive in this regime, and that these modes may have significantly longer damping times which would act to further increase their detectability.

Acknowledgments
We are indebted to Kostas Glampedakis for obtusely irreverent banter and occasional scientific insight. This work was supported by the SFB/Transregio 7 on "Gravitational Wave Astronomy" by the DFG. PL was supported by the Alexander von Humboldt Foundation. Computations were performed on the Multi-modal Australian ScienceS Imaging and Visualisation Environement MASSIVE (www.massive.org.au).

References

[1] Baggio L, Bignotto M, Bonaldi M, Cerdonio M, Conti L, de Rosa M, Falferi P, Fortini P, Inguscio M, Liguori N, Marin F, Mezzena R, Mion A, Ortolan A, Prodi G A, Poggi S, Salemi F, Soranzo G, Taffarello L, Vedovato G, Vinante A, Vitale S and Zendri J P 2005 *Phys. Rev. Lett.* **95** 081103
[2] Abbott B and et al 2007 *Phys. Rev. D* **76** 062003
[3] Abbott B and et al 2008 *Phys. Rev. Lett.* **101** 211102
[4] Modestino G and Pizzella G 2011 *Phys. Rev. D* **83** 062004
[5] Abadie J and *et al* 2011 *Astrophys. J.* **734** L35
[6] Ioka K 2001 *Mon. Not. R. Astron. Soc.* **327** 639
[7] Corsi A and Owen B J 2011 *Phys. Rev. D* **83** 104014
[8] Levin Y and van Hoven M 2011 *Mon. Not. R. Astron. Soc.* **418** 659
[9] Zink B, Lasky P D and Kokkotas K D 2012 *Phys. Rev. D* **85** 024030 arXiv:1107.1689
[10] Ciolfi R, Lander S K, Manca G M and Rezzolla L 2011 *Astrophys. J.* **736** L6 arXiv:1105.3971
[11] Lasky P D, Zink B, Kokkotas K D and Glampedakis K 2011 *Astrophys. J.* **735** L20
[12] Zink B, Schnetter E and Tiglio M 2008 *Phys. Rev. D* **77** 103015
[13] Korobkin O, Abdikamalov E B, Schnetter E, Stergioulas N and Zink B 2011 *Phys. Rev. D* **83** 043007 arXiv:1011.3010
[14] Zink B 2011 HORIZON: Accelerated General Relativistic Magnetohydrodynamics arXiv:1102.5202
[15] Antón L, Zanotti O, Miralles J A, Marti J M, Ibánez J M, Font J A and Pons J A 2006 *Astrophys. J.* **637** 296
[16] Anderson M, Hirschmann E W, Liebling S L and Neilsen D 2006 *Class. Quantum Grav.* **23** 6503
[17] Lasky P D, Zink B and Kokkotas K D 2012 in Preparation
[18] Bocquet M, Bonazzola S, Gourgoulhon E and Novak J 1995 *A&A* **301** 757
[19] Markey P and Tayler R J 1973 *Mon. Not. R. Astron. Soc.* **163** 77
[20] Lander S K and Jones D I 2011 *Mon. Not. R. Astron. Soc.* **412** 1730
[21] Braithwaite J 2007 *A&A* **469** 275
[22] Braithwaite J and Nordlund A 2006 *A&A* **450** 1077
[23] Braithwaite J 2009 *Mon. Not. R. Astron. Soc.* **397** 763
[24] Yoshida S, Yoshida S and Eriguchi Y 2006 *Astrophys. J.* **651** 462
[25] Ciolfi R, Ferrari V, Gualtieri L and Pons J A 2009 *Mon. Not. R. Astron. Soc.* **397** 913
[26] Lindblom L and Detweiler S L 1983 *Astrophys. J. S.* **53** 73
[27] Andersson N and Kokkotas K D 1998 *Mon. Not. R. Astron. Soc.* **299** 1059
[28] Sathyaprakash B S and Schutz B F 2009 *Living Rev. Relativity* **12** 2